Hydroxyl Tagging Velocimetry Demonstration in an Augmented Spark Igniter

Thomas P. Jenkins[1]
MetroLaser, Inc., Laguna Hills, California

Marsalis Pullen[2] and Robert W. Pitz[3]
Vanderbilt University, Nashville, Tennessee

Darren C. Tinker[4]
NASA Marshall Space Flight Center, Huntsville, Alabama

and

Robin J. Osborne[5]
ERC, Inc., Jacobs Space Exploration Group, Huntsville, Alabama

Hydroxyl tagging velocimetry (HTV) involves tagging a flow by "writing" a line of OH molecules using a laser beam to dissociate H_2O molecules and capturing an image of the line after a short delay using laser-induced fluorescence. Velocity is obtained by a time-of-flight analysis of the data. In this effort, HTV was used for obtaining both instantaneous and average velocity profiles in the flow of an augmented spark igniter. Two modes of camera readout were investigated, called conventional full-frame mode and dual image feature (DIF) mode. In DIF mode, two images are captured in quick succession and therefore the measurement has low sensitivity to vibration. Measurement uncertainty for the DIF case varied from 3% at the centerline to 10% at the edges of the profile in a 1000-m/s flow. For the full-frame case, measurement uncertainty varied from 3% at the centerline to 7% at the edges. This demonstration provides evidence that the HTV technique is well suited for obtaining velocity profiles in the challenging environment of either a rocket engine or rocket engine igniter.

I. Nomenclature

ASI	=	augmented spark igniter
b	=	*y*-intercept of linear fit of HTV tag line,
DIF	=	dual image feature
HTV	=	hydroxyl tagging velocimetry
ICCD	=	intensified charge coupled device
m	=	slope of linear fit to OH tag line
SNR	=	signal-to-noise ratio
x	=	horizontal coordinate of HTV image
y	=	vertical coordinate of HTV image
σ	=	standard deviation of displacement in tag line

[1] President and Chief Technical Officer, MetroLaser, AIAA Associate Fellow.
[2] Graduate Student, Mechanical Engineering, AIAA Student Member.
[3] Professor, Mechanical Engineering, AIAA Fellow.
[4] Combustion Engineer, NASA, AIAA Member.
[5] Subject Matter Expert, ERC, Inc., Jacobs Space Exploration Group, AIAA Associate Fellow.

II. Introduction

Current space exploration interests are returning to the Moon as well as a manned mission to Mars. Extensive development and testing of rocket engines are needed to achieve these goals and improved measurement methods are desired. Exhaust velocity is a critical parameter for characterizing rocket engine performance [1,2,3], yet few methods exist for performing plume velocity measurements due to the hostile high-temperature environment. Accurate measurements of plume conditions are essential for anchoring computer models that are needed to reduce development costs of present and future engines.

Traditional methods of measuring flow velocities are not suitable for rocket plumes because of the extreme temperatures and velocities. Physical probes such a pitot tubes or hot wires may quickly erode. Conventional laser velocimetry techniques, such as particle imaging velocimetry and laser Doppler velocimetry, are challenged as well due to a lack of sufficient seed particles, large background emission levels, beam steering due to shock waves and severe turbulence, and extreme acoustic noise [4,5]. Particles that could be used for velocity techniques may exist naturally, but they are typically low in number concentration, and their concentrations may be unreliable [6]. In addition, at velocities of rocket plumes, which can be thousands of meters per second, particle motion is often not a good representation of fluid motion due to particle lag [5,7,8]. In this paper, we demonstrate a laser velocimetry method for high-speed flows related to rocket engines that does not rely on particles.

Hydroxyl tagging velocimetry (HTV) was developed at Vanderbilt University for characterizing flows that contain H_2O via photodissociation of vibrationally exited H_2O into OH and H molecules [9, 10]. Because it does not rely on particles and the OH tag persists at high temperature, it is especially well suited for high-speed high-temperature flows.

Because H_2O is naturally present as a combustion product in the plumes of hydrogen- and hydrocarbon-fueled rockets, the method is attractive for studying the exhaust flow from these types of engines [11]. OH lifetimes are typically on the order of microseconds or longer for most of the combustion conditions relevant to rocket engine environments (i.e., fuel-rich, near stoichiometric) [6]. Here we demonstrate the technique in methane-oxygen combustion products issuing from an augmented spark igniter (ASI).

III. Technique

A conceptual drawing of the HTV technique applied to an ASI is shown in Figure 1. In step 1, a pulse from a 193-nm laser is focused to write a line of OH into the flow by dissociating H_2O. In step 2, the tagged region of the flow is interrogated by a second pulse from a 283-nm laser after a finite delay. The 283-nm beam is formed into a sheet that overlaps with and excites fluorescence from the OH tagged line. A planar image of this fluorescence pattern is captured by an intensified charge coupled device (ICCD) camera at a wavelength band centered at 308 nm. A filter with a center wavelength of 310 nm and FWHM bandpass of 10 nm was used to reject background radiation from combustion in the measurement zone that might otherwise interfere with the measurement of the tag lines. In step 3, raw images of the fluorescence are processed to obtain velocities in the flow by curve fitting the observed tag lines to obtain the displacement between the read and write pulses and performing a time-of-flight analysis. The result is an instantaneous, spatially resolved velocity measurement. The main components are the read laser, write laser, camera, beam steering optics, and collection optics.

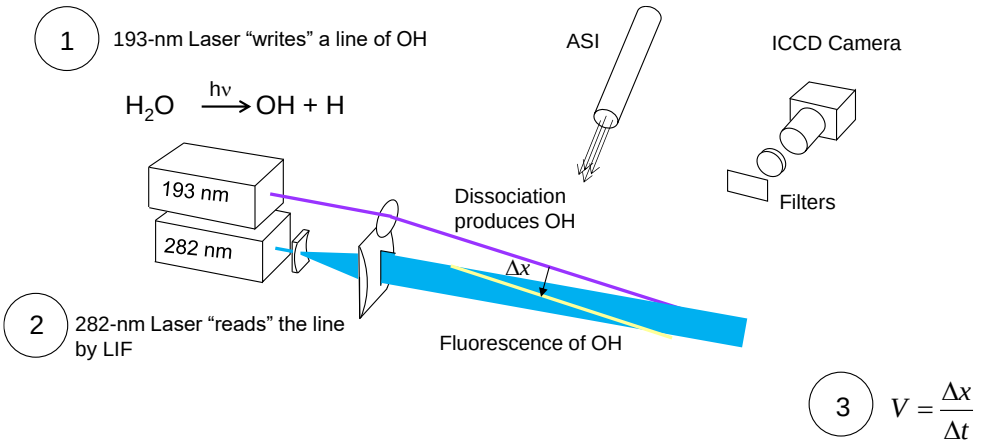

Figure 1. Hydroxyl tagging velocimetry applied to an augmented spark igniter.

.

IV. Experimental

The HTV measurement system consisted of two laser systems, a camera, and various optics. These were arranged to perform measurements on a rocket engine igniter test article. A description of the HTV measurement system is given below in section A and a description of the test article is given in section B. Discussion of the processing methods, hardware, software, diagnostic tools, services, etc. used in this paper is solely for informational purposes and not an endorsement by the authors, their employers, or the publisher.

A. HTV Measurement System

The optical system consisted of mirrors and lenses to deliver the 193-nm write laser beam and the 283-nm read laser sheet and to the measurement zone. A diagram of the HTV system is shown in Figure 2. The 193-nm beam was produced by an excimer laser (Lambda Physik COMPex 150), focused to a diameter of approximately 1 mm at the measurement location. The read laser consisted of a dye laser (Continuum Vista) pumped by a pulsed Nd:YAG laser (Continuum Powerlite 9010) at 532 nm with a pulse energy of about 350 mJ. The fundamental output beam of the dye laser had a wavelength of 566 nm and was produced using Rhodamine 590 dye, which was sent into a second harmonic generator (SHG) to produce the read laser wavelength of 283 nm, suitable for exciting fluorescence from OH radicals in the flow. The 283-nm read laser beam was formed into a sheet approximately 6 mm in height and 0.5 mm in thickness and directed across the exit of the ASI test article. This arrangement allowed the 266-nm sheet to be coincident with the interrogating line of OH created by the write laser at 193 nm. Planar laser-induced fluorescence images of OH were obtained with an intensified charge coupled device (ICCD) camera (Princeton Instruments PIMAX4) using a UV lens (Nikkor 105-mm f/4.5 UV). A 10-nm bandpass filter centered at 310 nm (Edmund Optics #34-980) was used on the camera lens to block all light except the OH fluorescence.

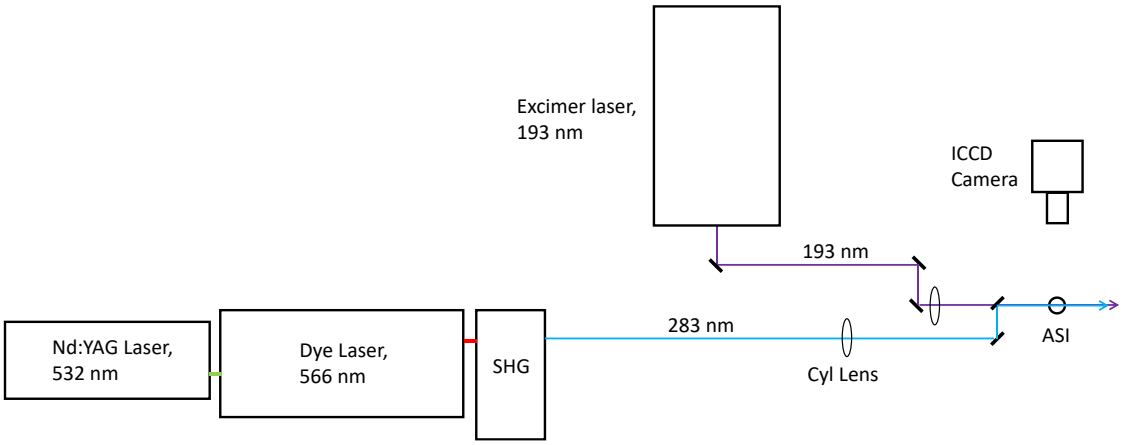

Figure 2. Experimental layout of the HTV measurement system.

The 283-nm sheet was directed horizontally across the jet, centered 14 mm above the exit, which was approximately 12 mm in diameter. The 193-nm write beam was directed to lie within the plane of the laser sheet, as shown in Figure 3, at an angle of 15° to the horizontal. The ICCD camera imaged the laser sheet from a distance of 0.42 m normal to the sheet.

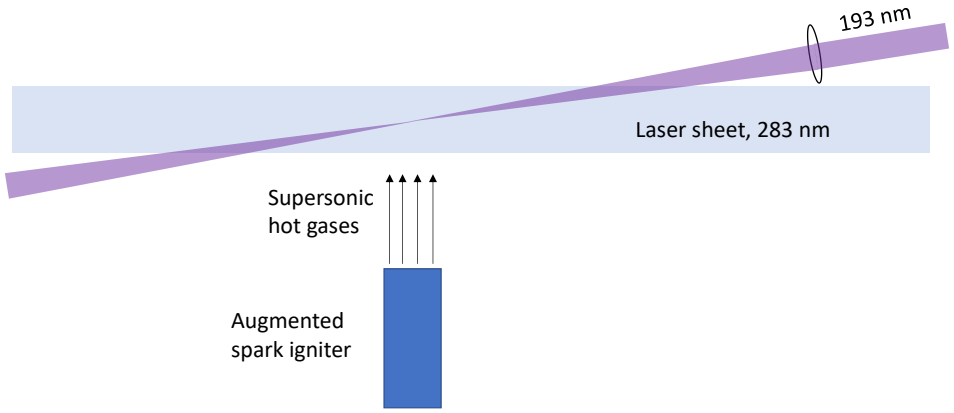

Figure 3. Laser beam and sheet intersection for HTV on an augmented spark igniter.

B. Test Article: Augmented Spark Igniter

The ASI test article selected for this HTV demonstration can be a critical component of a space mission since it can determine not only the success of the mission but also the safety of the crew. Ignition of a liquid rocket engine involves producing a series of electric discharges (sparks) though a mixture of fuel and oxidizer gases within the small ASI chamber [12,13]. The mixture ratio of the gases must be within the range of flammability during the limited window of time that sparking occurs. Once the propellants in the ASI are successfully lit, the resultant combustion gases travel through a torch tube to light the larger flow of propellants in the main combustion chamber of the liquid rocket engine.

The ASI chosen as the test bed for our HTV system was a NASA device that was investigated in a parallel effort with other diagnostics [14,15,16,17]. A conceptual diagram with approximate dimensions of the exit plane of the ASI torch tube with its outer annulus is shown in Figure 4. The combustion products from a lean methane-oxygen mixture flow from the central tube while pure methane flows through the outer annulus. At some distance downstream of the torch tube, the annular flow of pure methane is expected to mix and burn with the exterior portion of the lean combustion products exiting from the core flow, creating an even hotter diffusion flame around the core flow. Recent experiments involving schlieren imaging with flowing oxygen have enabled the temporal and spatial characteristics of the upstream spark discharge over a range of flow conditions and gap geometries [15]. The velocity measurements to be described in this current research were made downstream of the ASI torch tube using HTV to characterize the flow.

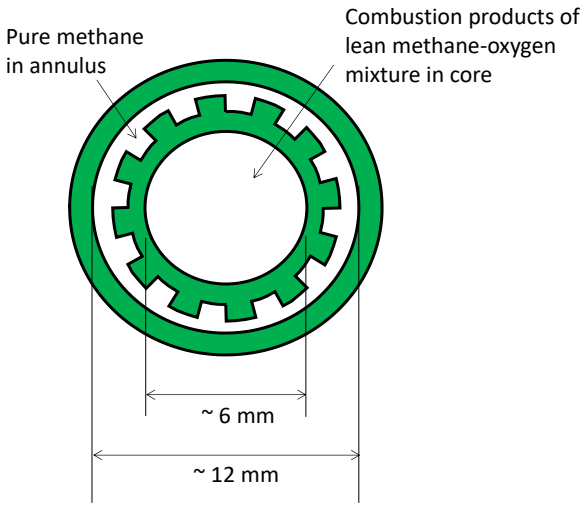

Figure 4. Conceptual drawing of exit plane of ASI

Figure 5. ASI in operation

V. Results and Discussion

A. Velocity Profiles

Spatially resolved measurements of velocity were obtained from the raw data taken in the ASI flow by assuming that the direction of motion was confined to the flow axis, which is the vertical axis of the images. This is a reasonable approximation since the measurements were taken near the jet exit in the core flow, where the streamlines should be essentially parallel with the axis of the jet in this high-speed flow. A computer program written in Matlab was used to process the data to compute velocities using a one-dimensional time-of-flight analysis. Briefly, the code fits a straight line to the undelayed image and uses this as a reference to compute velocity from the delayed image assuming vertical displacements. The code generates a line representing the tagged region of the delayed image based on a Gaussian fit in the vertical dimension to obtain the peak location for each column of pixels.

An example case is shown in Figure 6, which contains plots from the graphical user interface of the 1D MTV code written in Matlab. In part (a), a frame-averaged image of the undelayed tag line is shown with the linear curve fit to the data displayed as a yellow dashed line. Part (b) shows the frame-averaged delayed image corresponding to a 2-μs delay. The red line in part (b) is the deformed line obtained by curve fitting each column of pixels to a Gaussian function near the tagged region and obtaining the maximum of each Gaussian. Both frame averaged and instantaneous images were processed this way to obtain velocity profiles for two flow conditions of the ASI, one more fuel rich than the other. The case presented in Figure 6 was the rich condition.

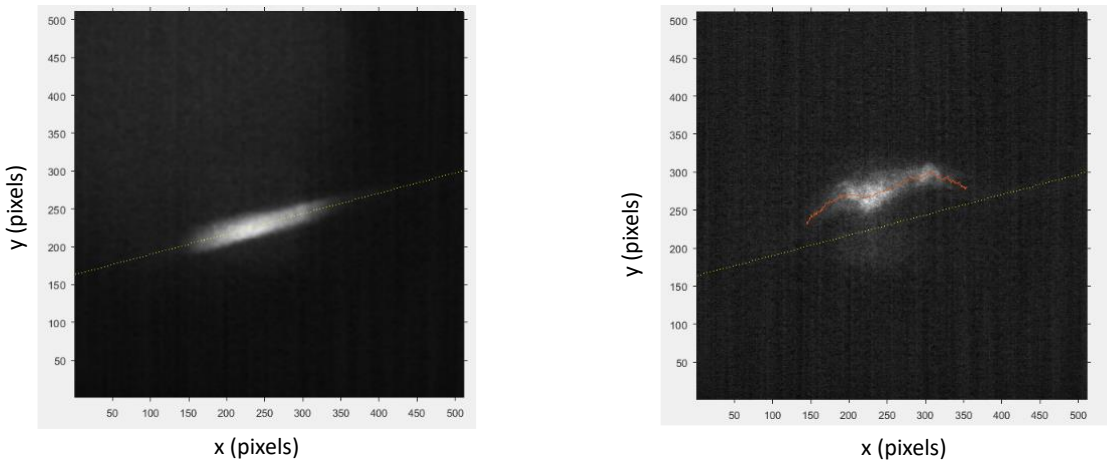

(a) Undelayed image (b) Delayed image

Figure 6. Raw images obtained using full-frame mode in the ASI flow, rich condition, showing (a) the frame-averaged undelayed image, and (b) the frame-averaged image after a delay of 2 μs.

Velocity profiles obtained from four experimental runs at the rich condition, including the run shown in Figure 6 (Test 17), are shown in Figure 7. The center of the profile corresponds to a height of 13.9 mm above the nozzle. However, since the write beam was at an angle of 15° with respect to the horizontal, the height of the measurement location varied from 11.6 mm above the nozzle exit plane on the left side of the image to 16.2 mm above it on the right side. Since the diameter of the tag line is about 1 mm, the spatial variations in velocity along the horizontal axis have been smoothed with a spatial cutoff frequency of 1 mm^{-1} to be consistent with the spatial resolution in the vertical dimension. The profiles from run to run can be seen to be consistent and all runs for the rich condition exhibit a dual-peak profile. The shape of the profile indicates acceleration in the annular shear layer where lean combustion products from the core flow mix with fuel flowing through the outer annulus, where high reaction rates are expected. The peak magnitudes are seen to be as high as 1400 m/s, with the flow on the centerline being 800 to 1000 m/s. Some variability in the velocity magnitudes of the peaks can be seen from run to run, but the magnitudes for a given run are consistent on both sides of the centerline.

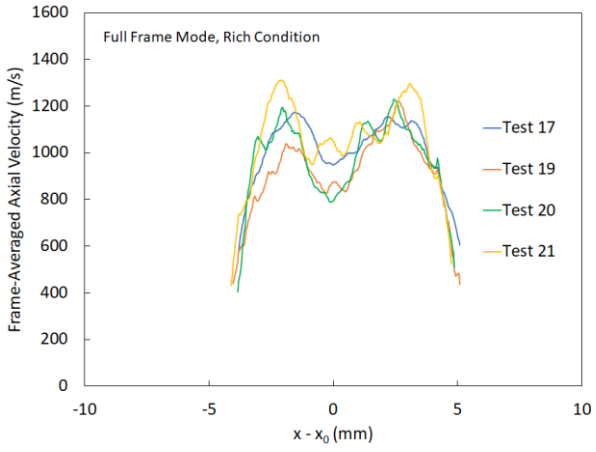

Figure 7. Frame-averaged velocity profiles obtained in the ASI flow for four runs at the rich condition.

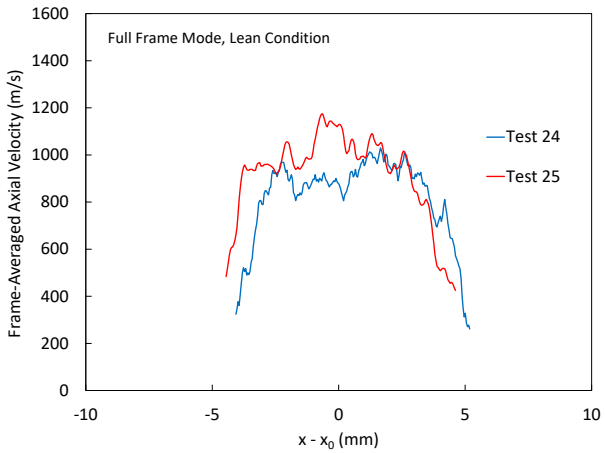

Figure 8. Frame-averaged velocity profiles in the ASI flow for two runs at the lean condition.

Velocity profiles from frame-averaged images obtained at the lean condition are shown in Figure 8. These profiles are also consistent from run to run but they have a different shape than those of the rich condition, as the strong peaks in the shear layer are absent and the profile is much flatter. Also, the velocities are seen to be somewhat lower than for the rich condition, with a maximum of about 1200 m/s.

Five velocity profiles obtained for the rich condition on a per-laser-shot basis are shown in Figure 9 and another five from the same run are shown in Figure 10. The image acquisition rate was limited by the laser and was 10 Hz, corresponding to a frame-to-frame interval of 100 ms. Since the laser pulse duration was 10 ns and the camera gate width was 200 ns, these profiles can be considered instantaneous. The total steady-state run time of the ASI was about 2 seconds for this run, during which about 20 profiles were obtained. The instantaneous profiles show more variability than the averaged profiles, both in spatial distribution and magnitude. This is to be expected since the flow is highly turbulent.

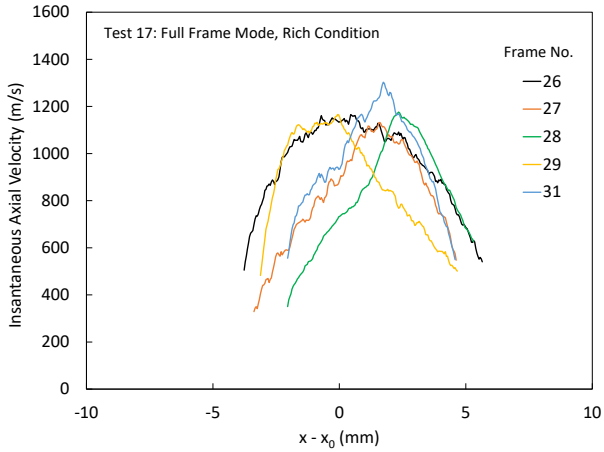

Figure 9. Instantaneous velocity profiles of frames 26 – 29 and 31 of Test 17 obtained with the camera in full-frame mode in the ASI flow for the rich condition.

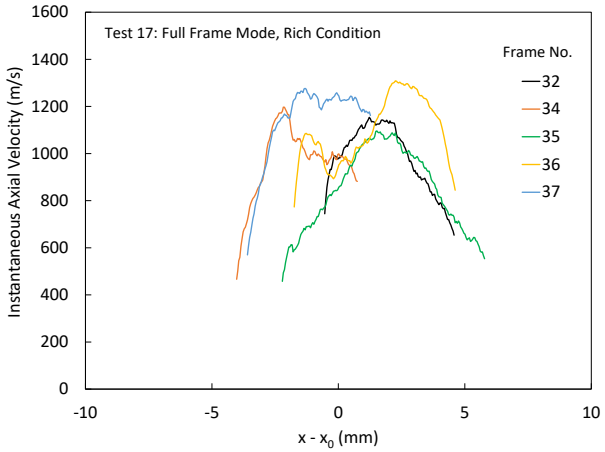

Figure 10. Instantaneous velocity profiles of frames 32 and 34 – 37 of Test 17 obtained with the camera in full-frame mode in the ASI flow for the rich condition.

B. Uncertainty Analysis

An analysis was performed based on using the uncertainty of the zero-delay line to estimate the uncertainty of the velocity measurement. This differs from other methods to measure the uncertainty in molecular tagging velocimetry (MTV) that are based on measuring a uniform velocity flow with MTV and assuming any variation from the uniform velocity value is the uncertainty [18].

The shot-to-shot variation in line fits were obtained for a given series of zero-delay images similar to that of Figure 6 (a) for 25 frames of an experimental run in the ASI flow. The horizontal range selected of pixel 150 to pixel 400 was based on what part of the image significant signals were observed. Images obtained in both full-frame and DIF camera readout modes were analyzed. In both cases, the spread in y-values was found to be greater at the edges of the range, which follows from the fact that the signal is lower there.

The variation in displacement due to the fits can be characterized by the standard deviation of the fit as a function of the x-coordinate. The standard deviation for a given x-value is defined as

$$\sigma(x) = \sqrt{\langle (y - \langle y \rangle)^2 \rangle} \tag{1}$$

where y is the fitted line for a given zero-delay frame, given by

$$y = mx + b \tag{2}$$

where m and b are the slope and intercept, respectively. The angle brackets in Equation (1) indicate the mean over all frames. Substituting Equation (2) into Equation (1), carrying out the multiplication, and simplifying, we get

$$\sigma(x) = \sqrt{\langle m^2 \rangle x^2 + 2\langle mb \rangle - \langle m \rangle^2 x^2 - 2\langle m \rangle \langle b \rangle x + \langle b^2 \rangle - \langle b \rangle^2}. \tag{3}$$

Equation 3 was used to compute the standard deviation in the fit as a function of x for this case. The results are shown for both camera readout modes in Figure 11**.**

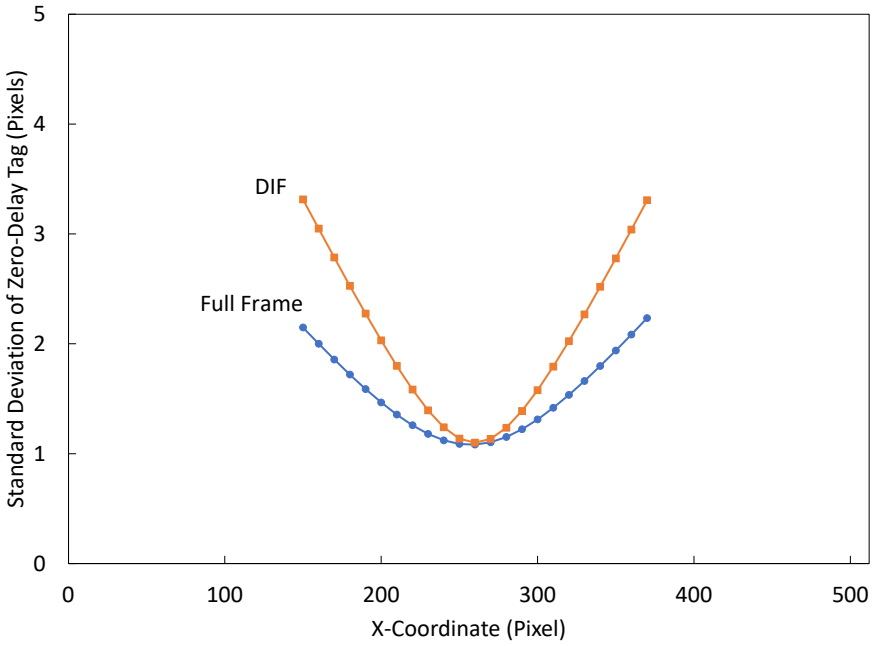

Figure 11. Standard deviation in the linear fit to the zero-delay tag line for HTV images obtained in the ASI flow for the rich condition, comparing full-frame and DIF readout modes.

Figure 11 shows the same standard deviation of 1.1 pixels in the center of the profile for both camera readout modes. However, it increases significantly toward the edges of the profile for both modes, and more so for the DIF mode than the full-frame mode. In general, the signal intensities in the DIF images were about 40% lower than for the full-frame images due to the shorter readout time, leading to a lower signal-to-noise ratio (SNR). Over the useful x-coordinate range, the displacement error is within 2.2 pixels for the full-frame case and within 3.3 pixels for the DIF case. For this experimental setup, the scaling factor was 43 μm/pixel in both the x and y directions. This corresponds to an error in the zero-delay tag line of 47 μm, 95 μm, and 142 μm for the centerline, edge with full-frame, and edge with DIF cases, respectively.

The displacement errors for the delayed tag lines are not as straightforward to compute. As a first approximation, we assume they are the same as for the undelayed lines. In this case, for a 2-μs delay, the corresponding velocity errors are given in Table 1. The advantage in measurement precision for the full-frame mode should be weighed against the benefits of immunity to vibration for DIF mode. For the present ASI test article, it was obvious that vibration was not an issue, as the line fits to the undelayed images revealed that there is little variation from shot-to-shot.

Table 1. Estimated HTV errors in the ASI flow for a 2-μs delay.

	Velocity error at centerline (m/s)	Velocity error at edges (m/s)
Full-frame mode	34	66
DIF mode	34	99

The velocities measured in the present experiments were on the order of 1000 m/s, so the estimated errors of 34, 66, and 99 m/s in **Table 1** correspond to about 3%, 7%, and 10% of this value. These uncertainties may be considered reasonable for a high temperature supersonic flow that is difficult to probe experimentally. However, the uncertainty could be improved by reducing the diameter of the write beam. The 1-mm diameter in the current experiments was

relatively large compared to the fluid dynamic scales, which hinders the measurement in two ways. First, if the laser energy is spread out over a large cross-sectional area, the intensity tends to be less than ideal, resulting in a low fraction of H_2O molecules being dissociated and thus a low OH tag concentration. Second, the uncertainty in the position of the tag line is directly proportional to the width of the line, thus a smaller diameter leads to better measurement precision. In the current effort, it was not possible to focus the beam to a diameter of less than 1 mm due to the large divergence of our aging laser. Future researchers would be well advised to use a write beam that can focus a beam to less than a few hundred microns. A typical commercially available excimer laser has a beam divergence of less than 1 mrad, in which case for our setup the diameter of the write beam would have been less than 300 μm, which would have greatly improved the measurement precision.

The ability to locate an MTV line is also directly related to the SNR of the line measured. Previous work has shown that one needs at least an SNR of 4 to locate the MTV line and more than 4 does not give much improvement [19,20]. In the current research, SNR values were limited primarily by background OH and low signal levels and were generally less than 4, often being on the order of 2 or less. The 1.1-pixel uncertainty obtained in Figure 11 is consistent with the findings of Ramsey and Pits [20], who reported uncertainties of 0.5 pixels for SNR values of around 2.

VI. Conclusion

A version of hydroxyl tagging velocimetry has been developed for application to liquid rocket engine exhausts. A prototype HTV system was designed, constructed, and demonstrated in the flow from an augmented spark igniter. The system consisted of a 193-nm write laser pulse that produces a line of OH molecules to tag the flow by dissociating H_2O molecules, which are typically present in the exhaust of a liquid rocket engine as well as many other combustion devices. The tagged line is interrogated a few microseconds later by a 283-nm read laser pulse in the form of a light sheet that is imaged by a gated camera. Laser-induced fluorescence from the tag line of OH provides a marker of the flow, from which the displacement can be measured to obtain velocity. Using two laser systems, a gated camera, and optics, both instantaneous and averaged velocity profiles were obtained in the ASI flow for both rich and lean operating conditions. Two modes of camera readout were investigated, including the conventional full-frame mode, in which one image was obtained every 100 ms, and dual image feature mode, in which pairs of images having a separation of as little as 1.5 μs were obtained every 100 ms. It was found that in DIF mode the signal was reduced compared to full-frame mode, resulting in a lower signal-to-noise ratio. This led to a greater measurement uncertainty for the DIF case, which varied from an estimated 34 m/s at the centerline to 99 m/s at the edges of the profile. In comparison, the full-frame case was found to have a measurement uncertainty varying from 34 m/s at the centerline to 66 m/s at the edges. Although DIF mode resulted in some reduction in measurement precision, it would be useful in applications where there is a high level of vibration, such as on a large rocket engine, since the undelayed and delayed images could be guaranteed to have the same spatial reference. However, vibration was not an issue for the ASI device test in this effort, thus full-frame mode was the preferred approach. Focusing of the write beam was limited by the large beam divergence of the 193-nm laser used, producing a beam waist of 1 mm diameter. A smaller waist should produce a greater OH tag concentration, leading to greater SNR and higher measurement precision. This demonstration provides evidence that the HTV technique is well suited for obtaining velocity profiles, both averaged and instantaneous, in the challenging environment of a rocket engine or rocket engine igniter.

Acknowledgments

The authors are grateful to NASA for sponsoring this work, which was performed under NASA Small Business Innovation Research contract number NN17CS04C and NASA Fellowship grant number NNX16AM57H.

References

[1] Huzel, D.K, and Huang, D. H., *Modern Engineering for Design of Liquid-Propellant Rocket Engines*, 2nd ed., American Institute of Aeronautics and Astronautics, Inc., Washington DC, 1992. https://doi.org/10.2514/4.866197.

[2] Sutton, G. P., and Biblarz, O., *Rocket Propulsion Elements*, 9th ed., John Wiley & Sons, Hoboken, 2017.

[3] Heister, S. D., Anderson, W. E., Pourpoint, T. L., and Cassady,J. R., *Rocket Propulsion*, 1st ed., Cambridge University Press, Cambridge, 2018. https://doi.org/10.1017/9781108381376

[4] Kugler, H. P., "Recent results in rocket exhaust anemometry," *Phys. Scr*., Vol. 19, 1979, pp. 447-452.

[5] Bitter, M., Scharnowski, S., Hain, R., and Kähler, C. J., "High-repetition-rate PIV investigations on a generic rocket model in sub- and supersonic flows," *Exp Fluids*, Vol. 50, 2011, pp. 1019-1030.

[6] Son, M., Armbruster, W., Hardi, J. S., and Oschwald, M., "Measuring the velocity field of a shear-coaxial, cryogenic flame in a high-pressure rocket thrust chamber," *Proceedings of the Combustion Institute*, Vol. 38, 2021, pp. 3389-3397.

[7] Williams, O. J. H., Nguyen, T., Schreyer, A. M., Smits, A. J., "Particle response analysis for particle image velocimetry in supersonic flows," *Physics of Fluids*, Vol. 27, 2015, 076101, 15 pages.
[8] Huffman, Jr., R. E., Elliott, G. S., "An experimental investigation of accurate particle tracking in supersonic, rarefied axisymmetric jets," AIAA Paper 2009-1265, January 2009.
[9] Wehrmeyer, J. A., Ribarov, L. A., Oguss, D. A., and Pitz, R. W., "Flame flow tagging velocimetry with 193-nm H_2O photodissociation", *Applied Optics*, Vol. 38, No. 33, 1999, pp. 6912-6917.
[10] Lahr, M. D., Pitz, R. W., Douglas, Z. W., and Carter, C. D., "Hydroxyl Tagging Velocimetry in Cavity-Piloted Mach 2 Combustor", AIAA Paper 2006-0040, January 2006.
[11] Ramsey, M. C., Pitz, R. W., Jenkins, T. P., Matsutomi, Y., Yoon, C., Anderson, W. E., "Planar 2D velocity measurements in the cap shock pattern of a thrust optimized rocket nozzle," *Shock Waves*, Vol. 22, 2012, pp. 39-46.
[12] Marshall, W. M., Osborne, R. J., and Greene, S. E., "Development of Augmented Spark Impinging Igniter System for Methane Engines," AIAA Paper 2017-4665, 2017. https://doi.org/10.2514/6.2017-4665
[13] Hurlbert, E. A., Moreland, R. J., and Candel, S., "Propellant Ignition and Flame Propagation," Liquid Rocket Thrust Chambers: Aspects of Modeling, Analysis, and Design, edited by M. Popp, J. Hulka, V. Yang, and M. Habiballah, Vol. 200, *Progress in Astronautics and Aeronautics*, AIAA, Reston, VA, 2004, pp. 405–436.
[14] Tinker, D. C., Osborne, R. J., and Pitz, R. W., "Examination of annular-electrode spark discharges in flowing oxygen – an overview," AIAA Paper 2018-4776, July 2018.
[15] Tinker, D. C., Pullen, M., Osborne, R. J., and Pitz, R. W., "Examination of annular-electrode spark discharges in flowing oxygen – experimental nuances," AIAA Paper 2019-0466, January 2019.
[16] Tinker, D. C., Pullen, M., Osborne, R. J., and Pitz, R. W., "Cylindrical air-gap electrode spark discharge characterization and quenching," *Journal of Propulsion and Power*, DOI: 10.2514/1.B38303, 2021, 11 pages.
[17] Tinker, D. C., "Compact Augmented Spark Igniters for Liquid Rocket Engines," Ph.D. Dissertation, Vanderbilt Univ., Nashville, 2021, http://hdl.handle.net/1803/16419
[18] Mustafa, M. A., Parziale, N. J., Smith, M. S., Marineau, E. C., "Nonintrusive freestream velocity measurement in a large-scale hypersonic wind tunnel," *AIAA Journal* Vol. 55, No. 10, 2017, pp. 3611-3616.
[19] Gendrich, C. P., Koochesfahani, M. M., "A spatial correlation technique for estimating velocity fields using molecular tagging velocimetry (MTV)," *Experiments in Fluids* Vol. 22, 1996, pp. 67-77.
[20] Ramsey, M. C., Pitz, R. W., "Template matching for improved accuracy in molecular tagging velocimetry," *Experiments in Fluids* Vol. 51, 2011, pp. 811-819.